UNIVERSITY OF CALIFORNIA, SAN DIEGO

Automated Quantification of Capillary Microhemodynamic Parameters from Intravital Microscopy Videos

A thesis submitted in partial satisfaction of the requirements for the degree

Master of Science

in

Bioengineering

by

John Allen Gruetzner

Committee in charge:

Professor Pedro Cabrales, Chair
Professor Marcos Intaglietta
Professor Geert Schmid-Schoenbein

2015

The Thesis of John Allen Gruetzner is approved and it is acceptable in quality and form for publication on microfilm and electronically:

Chair

University of California, San Diego

2015

Table of Contents

List of Figures

List of Tables

List of Supplemental Source Code

gruetzner_main.cpp

Acknowledgements

Many heartfelt thanks are given to Cynthia Walser and Froilan Barra for their preparation of the animals. Additionally, I am forever indebted to Daniel Ortiz and all members of the Cabrales Lab for their unwavering support and assistance. And to Professor Pedro Cabrales, of whose kindness I was not worthy, I have no words that could hope to adequately convey my gratitude.

ABSTRACT OF THE THESIS

Automated Quantification of Capillary Microhemodynamic Parameters

from Intravital Microscopy Videos

by

John Allen Gruetzner

Master of Science in Bioengineering

University of California, San Diego, 2015

Professor Pedro Cabrales, Chair

Microcirculatory aberrations have been implicated as a driving force in the pathogenesis of sepsis and other diseases, but have only recently come under scrutiny with the development of novel visualization techniques. The heterogeneity of the microcirculation necessitates that a thorough assessment of capillary hemodynamics requires large sample sizes, inhibiting manual analysis, but no method presently exists to analyze capillary flow velocity or hematocrit in an automated manner without

significant restrictions. A self-validating software application was developed that tracks capillary flow velocity and approximates capillary hematocrit from intravital microscopy videos, requiring minimal input from the user once calibrated. Additionally, data detailing the path taken by each successfully tracked cell may be stored, and the software outputs a copy of the input video with capillary outlines overlaid and with successfully tracked cells marked. In this manner, the user may choose to validate, accept, reject, and segregate the raw data as they wish.

I: Introduction

The Microcirculation and Disease

It has been estimated that sepsis affects at least 15 million people every year worldwide.[1] In the United States, sepsis commands the highest aggregate cost for all hospitalizations at over $20 billion per year.[2,3] Its progression to severe sepsis is often fatal, with patient mortality rates remaining as high as 29%, despite significant advances in the ability of hospital intensive care units to administer vital-organ support.[4,5]

Treatment of severe sepsis has long followed the 'VIP' approach,[6] with ventilate, infuse, and pump remaining core tenants in the present day.[7,8] This approach addresses harmful alterations in systemic parameters that occur during severe sepsis, but fluid resuscitation in standard practice has been demonstrated to leave microcirculatory beds hypoxemic despite adequate restoration of normal systemic hemodynamics.[9] In severe sepsis, it is often dysfunction at the microcirculatory level that results in disease progression.[10,11] Persistence of uncorrected microcirculatory aberrations is predictive of patient outcome in septic shock.[12]

The rheology of blood in the microvasculature under normal conditions has been a topic of study for many decades.[13] Unfortunately, the mechanisms responsible for altering microcirculatory flow throughout sepsis pathogenesis and in other diseases remain insufficiently investigated at the laboratory level. Considering the relative ease in which systemic measurements of blood flow are taken, when juxtaposed with the

relative difficulty of visualizing and assessing the state of the microcirculation, the focus on systemic parameters as markers of health is understandable. However, recent advancements in technology are slowly removing these barriers to understanding in the clinic and the laboratory, where further research will be necessary if meaningful changes are to be applied to treatment in the clinic.

Imaging Techniques

A number of techniques have arisen that allow for visualization of the microcirculation, though each presents its own merits and drawbacks.

Nailfold capillaroscopy was the first major method by which the microcirculation could be viewed non-invasively in a clinical setting. Utilizing reflected light microscopy and taking advantage of the relative ease by which nailfold capillaries may be accessed, microhemorrhage, morphological anomalies, and devascularization may be quantified.[14] Though finding significant use in rheumatology, this technique is limited to the nailfold capillary bed and image resolution is restricted to preserve portability on clinical devices.[15,16]

The introduction of orthogonal polarization spectral imaging presented a more robust method for clinical microcirculatory study, reflecting and transmitting polarized light in a manner that back-illuminates subcutaneous vessels.[17] This technique lifted clinical restrictions on the locations that microcirculatory data could be extracted from, finding use in cardiology, endocrinology, and dermatology.[18-20] However, flow of erythrocytes tends to blur the imagery and individual capillaries are difficult to

discern.[21] Additionally, the high power required of the light source limits clinical portability, and the applied pressure needed for visualization alters cell velocity.[22]

The latest major clinically applicable addition, sidestream dark field imaging, addresses some of these problems. Using a ring-based stroboscopic LED system to reduce motion blurring, the technique produces images of similar quality when compared alongside orthogonal polarization spectral imaging results, but provides superior contrast for capillaries and venular granularity.[23] The ability to produce high-caliber images, coupled with the low cost of the system and its portability, allow sidestream dark field imaging to present itself as the most useful tool presently available for clinical microcirculatory visualization, already finding use in anesthesiology and oncology.[24,25] As in orthogonal polarization spectral imaging, the pressure of the probe alters cell velocity, and limits on the number of frames able to be captured impair velocity measurements.[26]

Not subject to the restrictions imposed on clinical devices, microcirculatory imaging techniques in the laboratory are numerous, but intravital microscopy has emerged as the "gold standard" in terms of achievable microcirculatory resolution, finding use in biology, oncology, immunology, toxicology, ophthalmology, rheumatology, and virology, among other areas.[27-33] Intravital microscopy allows for the unparalleled observation of erythrocyte flow through capillaries and other small vessels *in vivo*, often performed in anesthetized and unanesthetized rodents such as mice and hamsters via the window chamber model.[34] Although this is not a technique that can be applied directly in the hospital setting, as clinical imaging modalities

continue to be developed and improve in quality, relevance of insight gained from intravital microscopy-based research increases.

Contemporary Microhemodynamic Analysis

While novel imaging techniques have facilitated an improvement in the quality and resolution of microcirculatory imagery, assessment of these images is not so straightforward. Two major manual methods of analysis have been employed in clinical practice for both orthogonal polarization spectral imaging and sidestream dark field imaging, while a number of software packages exist or are in the development stage. Techniques for assessing the state of microcirculatory beds tend to be labor-intensive, and even automated software packages for assessing microcirculatory vessel flow often require manual vessel alignment and specific vessel phenotypes.

The primary clinically applicable microcirculatory bed scoring system assesses perfused vessel density based on the number of vessels crossing three equidistant vertical and three equidistant horizontal lines superimposed over the image.[35] The number of vessels that cross these lines is divided by the total line length to calculate density. Flow is then categorized as absent (lack of flow for 20 seconds), present (continuous flow for 20 seconds), or intermittent (flow is absent at least 50% of the time). The proportion of perfused vessels is calculated and multiplied by vessel density to provide perfused vessel density, considered a good estimate of functional capillary density.[36] Small vessels under 20 μm are considered separately from larger vessels, and were found to provide reliable estimates of functional capillary density as

well.[37] Despite measuring a number of parameters with low inter- and intra-observer variability, this method fails to take erythrocyte velocity into account and is manually intensive to compute.

The alternative clinically applicable scoring system is the calculation of a microvascular flow index.[38] In the standard method, an image of a microcirculatory bed is divided into four quadrants and flow is rated as absent, intermittent, sluggish, or normal. Point values of 0, 1, 2, or 3 are respectively assigned to each quadrant, and the quadrants are averaged to produce the microvascular flow index. While this assessment is quick to perform and erythrocyte velocity is incorporated, the scoring system is ordinal, limiting the conclusions that may be drawn from changes in velocity. As in the previous scoring system, small vessels under 20 μm are considered separately from larger vessels, although the inter- and intra-observer reliability with the microvascular flow index is considered poor.[39] Other variants of segmentation exist to produce a microvascular flow index, although agreement among microvascular flow indexes found under differing means was found to be inadequate.[40]

With regard to software, a number of packages have been developed. The CapImage software system has been designed for use in intravital microscopy, orthogonal polarization spectral imaging, and sidestream dark field imaging, but its use is limited to straight vessel segments only.[41] The CapiScope software system is capable of orthogonal polarization spectral imaging analysis, measuring functional capillary density, vessel diameter, and flow velocity. Unfortunately, it requires a lack

of movement artifacts and needs very stable imagery.[42] Various alternative software applications and imaging algorithms exist to evaluate intravital microscopy vessel flow, but common to all of them are restrictions on capillary analysis, often requiring manual vessel alignment and specific phenotypes. There is no automated analysis software that specifically targets capillary flow and provides reliable velocity data without significant user input.

Hypothesis

Given that the microcirculation has been implicated as a driving force behind the pathogenesis of sepsis and other diseases, and given that current microcirculatory imaging analysis methods fail to adequately evaluate changes at the capillary level, and given the need for an automated method of assessment to account for the substantial heterogeneity seen in microvasculature beds, it is reasoned that a method of assessing capillary flow that addresses these concerns must be developed to further our understanding of microcirculatory alterations in response to the diseased state, and it is hypothesized that such a method can be developed with current technologies.

II: Methods

Animal Preparation

All procedures were conducted in accordance with the Guide for the Care and Use of Laboratory Animals set forth by the National Institutes of Health. Male Golden Syrian hamsters (Charles River Laboratories, Boston, MA) had their dorsal region fitted with a skinfold window chamber. All protocol was approved by the University of California, San Diego Institutional Animal Care and Use Committee. The surgical techniques utilized in animal preparation are described in detail elsewhere.[43] In brief, the animals were prepared for chamber preparation under anesthesia, with the chamber consisting of two titanium frames with a circular observation window 15 millimeters in diameter. Following hair removal, the dorsal skin was lifted up from the animal using sutures, and one side of the titanium frame was positioned in contact with the animal's dorsum. Following the window outline, one side of the skinfold was removed until a thin section of retractor muscle remained. The remaining titanium frame was embedded with a glass coverslip and used to seal the chamber. Animals were given two days to recover and assessed for signs of edema or bleeding. Animals were then re-anesthetized to implant an arterial catheter in the carotid artery and a venous catheter in the jugular vein. Tunneled beneath the skin, catheters were exteriorized at the dorsal side of the neck and secured to the chamber. Experiments were performed within 48 hours of catheter implantation, allotting a 24 hour recovery period beforehand.

Inclusion Criteria

Only animals with a weight above 55 grams and showing no signs of distress or complication were marked suitable for experimentation. Systemic parameters were also examined, with a heart rate greater than 320 beats per minute, a mean arterial blood pressure of more than 80 mmHg, and a systemic hematocrit above 45% being required for experimental inclusion.

Microvasculature Image Acquisition

The unanesthetized hamsters were placed in a retraining tube containing a longitudinal slot through which the window chamber could protrude and were secured to the stage of a BX51WI transillumination microscope (Olympus, New Hyde Park, NY) fit with a 40X water-immersion objective (NA 0.7) and a long-working-distance condenser. An effective pixel-width of 0.3 μm was achieved by placing an additional lens before the camera. A blue filter (Spectra Physics, #59820) was inserted before the light source. Prior to image acquisition, hamsters were allowed 20 minutes to adjust to their surroundings. Video footage was stored on an external hard drive for analysis.

Code Base

All software was written utilizing the C++ Standard Library in conjunction with the OpenCV Library. The OpenCV Library is available for academic and commercial use, copyrighted under the BSD 3-Clause License.

Parameter Optimization

A large number of adjustable parameters are provided for optimal calibration of the software by the user. Parameters related to erythrocyte detection and segmentation, along with their default values, are listed in **Table 1**. Parameters related to erythrocyte pathing analysis and hematocrit estimation, along with their default values, are listed in **Table 2**.

Table 1: Adjustable parameters for optimization of object detection and segmentation.

Parameter	Description	Default Value
Threshold Block Size	Block dimensions in pixels over which to perform thresholding across the image.	45
Threshold Constant	Constant intensity value added to pixels after thresholding.	0
Dilation-Erosion Strength	Dimensions of the kernel by which the image is dilated or eroded.	8
Area Upper Limit	Contours enclosing a number of pixels above this value will be discarded.	1000000
Area Lower Limit	Contours enclosing a number of pixels below this value will be discarded.	10
Long-to-Short- Side Ratio Upper Limits	Upper limits of the rectangular long-to-short-side ratio for segmenting regions into 1, 2, 3, 4, and 5 pieces, respectively.	2.3, 3.4, 4.4 5.3, and 6.1
Aggregated Ratio Constant	Value by which to increase each rectangular long-to-short-side ratio upper limit for segmenting regions into more than 5 pieces.	0.7

Table 2: Adjustable parameters for optimization of pathing and hematocrit analysis.

Parameter	Description	Default Value
Maximum Cell Path Pixel Distance	Pixel distance under which cell center points must be between frames to associate them.	10
Maximum Cell Mask Pixel Distance	Pixel distance under which contour center points must be between frames to associate them.	20
Minimum Frames of Persistence	Minimum number of consecutive frames an object must be identified for to preserve tracking data.	50
Capillary Dilation	Dimensions of the kernel by which cell path lines are dilated for capillary boundary identification.	20

Upon initiation of video analysis, users are given a control panel with which to adjust parameters whilst observing the results of their adjustments in real-time as the video loops in the background. The nature of the input video will dictate how optimal calibration proceeds.

Video Pre-Processing

As the first step towards erythrocyte detection, each frame of the input video is subjected to a series of transformations to ensure analysis proceeds optimally. The border of each video frame is given a 20-pixel thick buffering region of black pixels to

prevent edge artifacts throughout the analysis. To eliminate the interference of visual artifacts outside of the field of view, a copy of each frame is converted to a grayscale image and blurred using a kernel dimension size of two. The pixels of an intensity higher than zero, predominantly located within the field of view, are then set to the maximum value of 255 via a thresholding procedure and an erosion operation is performed, convoluting the image with a kernel size of 15 and retaining the minimum pixel intensity at the kernel anchor point to eliminate any remaining noise in the region outside the field of view. This image is then saved to be later compared with the frame it was copied from for elimination of artifacts (pixels with an above-zero intensity) beyond the field of view. The original video frame is then converted to a grayscale image for thresholding.

Thresholding

To segregate cells from their surroundings, an adaptive thresholding maneuver is performed that takes potential lighting and contrast gradients into account. The image is blurred using a kernel dimension size of 5, and thresholding occurs with a pixel block size dictated by the user, imparting a threshold value of the weighted sum (cross-correlation with a Gaussian window) of the squared block size neighborhood. This permits erythrocytes to contrast against their immediate surroundings for segregation, even though lighting conditions may cause image intensity to vary significantly across the field of view. The mask created during pre-processing is then applied to eliminate artifacts outside the field of view, and an erosion-dilation

operation is performed with a kernel size dictated by the user to eliminate noise within the field of view.

Contour Detection

Utilizing an algorithm developed by Satoshi Suzuki and Keiichi Abe, the contours of the erythrocytes are found by detecting the stark gradient changes created with the thresholding operation.[44] The image points making up the border of each contour are stored along with the total number of enclosed contour regions detected.

Contour Segmentation

Contours of interest outline single erythrocytes and clumped groups of erythrocytes. For each group of contour points, a rectangular bounding box that encloses all points and possesses the smallest area is found and stored in the form a center point, length, width, and angle of rotation. The rectangular area and the ratio of the longest-to-shortest side was calculated for each bounding box as well. Contours are discarded if their area is deemed too large or too small, according to user-selected values, in order to reduce noise and the interference of image artifacts. Should the user wish to segregate clumped erythrocytes, the long-to-short-side ratio of the bounding rectangles provides a parameter that the user may segment them with. For long-to-short-side ratios that approach the user-set limits, segmentation by the long-to-short-side ratio takes the segmentation of the previous frame's contours into account if the contours are found to have an area difference of less than 5% and their center points are within a user-specified number of pixels. The contours belonging to the inner rectangles of the segmented image are then given new rectangular bounding

boxes used to approximate cell positions. An ellipse is fit within these new bounding boxes and can be overlaid on the screen so that the user may verify how clumped contour regions are being divided. As before, ellipses with areas deemed too large or too small may be discarded based on user-selected parameters. The total number of remaining ellipses is stored as a preliminary estimate of detected cell count.

Cell Path Detection

The center points of all ellipses across all frames are stored so that the paths taken by individual cells may be found. Starting from the initial video frame, all ellipse center points are checked against those of the subsequent frame and associated with one another if they fall within a pixel distance set by the user. Cells can only belong to one cell path and are not checked against cells already associated with a cell path. By proceeding likewise through all frames of the video and storing in a separate vector the frame on which each new cell path is initiated, a map of all cells and their travels is found. Cell paths that are found to be shorter than a user-set number of frames are discarded, serving to further eliminate noise and unreliably tracked cells from analysis. The total length in pixels traveled by a cell is calculated with a simple smoothing algorithm to eliminate noise arising from changes in the position of the cell's center points. Both horizontal and vertical components of the center point coordinates in each cell are averaged with that of their preceding and subsequent frame coordinate components, if applicable. Should this not eliminate path noise to a

satisfactory level, the user may apply more robust smoothing algorithms to the raw pathing data.

Capillary Segregation

For purposes of capillary identification, the lines along which all cells were successfully found traveling are stored in an image matrix. These lines are then dilated by a user-specified value to produce an estimation of the profile belonging to capillaries of interest. The contours of these lines are found for later use in area and hematocrit calculations. The first point in which each cell path is initiated is then checked to see which capillary segment it falls within, so that data may be segregated by capillary. Additionally, the area taken up by all cells within a capillary contour, whether successfully tracked or not, is determined based on their prior thresholded profiles for purposes in capillary hematocrit estimation.

III: Results

What follows is a selection of images depicting visually the information that the software utilizes, processes, and returns. **Figure 1** represents sample input fields of view. **Figure 2** displays the outcome of the thresholding procedures. **Figure 3** displays the resulting contour lines superimposed upon the original input images. **Figure 4** depicts the bounding boxes used to segment clumped cells. **Figure 5** depicts the results of segmentation. As configured, users are able to switch between the viewpoints depicted in **Figures 1, 2, 3,** and **5** while parameters are adjusted within a control panel. **Figure 6** depicts the capillary mask used in hematocrit estimations. **Figure 7** depicts frames from the output video file, with successfully tracked cells marked and capillaries numbered for sorting purposes.

Thresholding

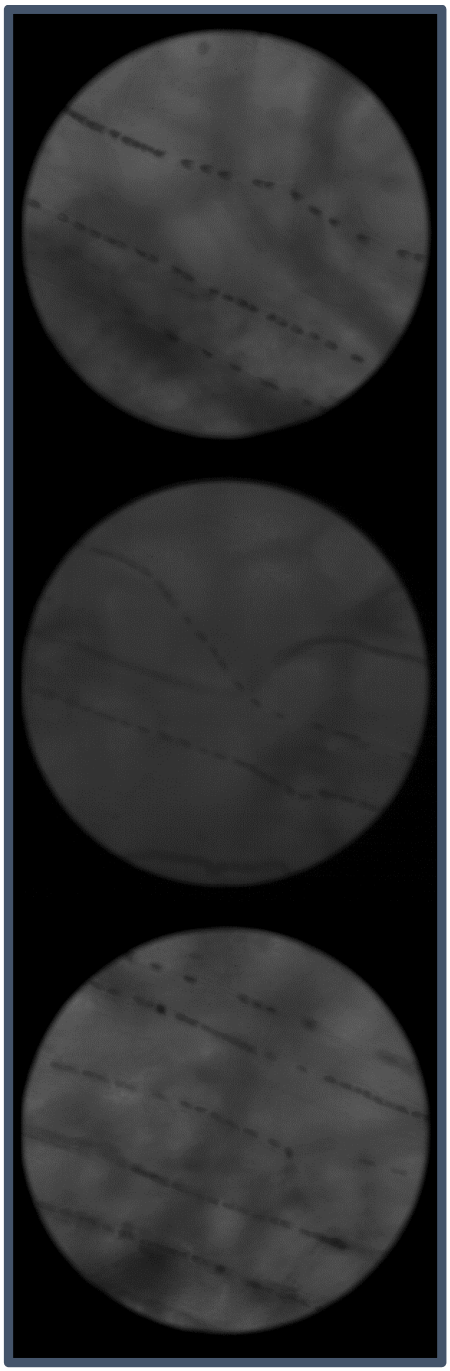

Figure 1: Sample video frames prior to modification and processing.

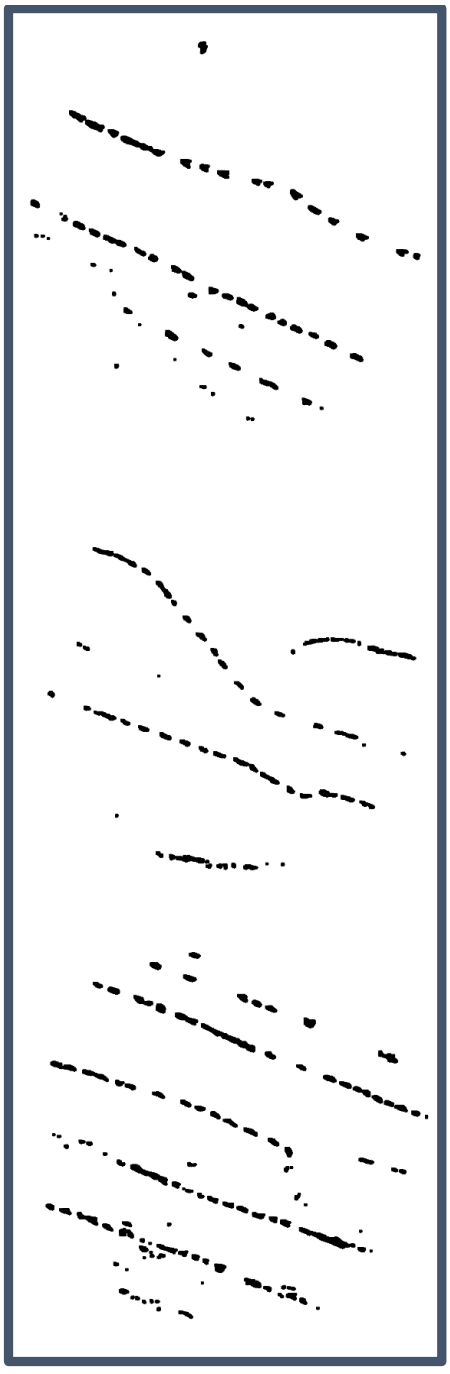

Figure 2: Video frames post-thresholding.

Contour Detection

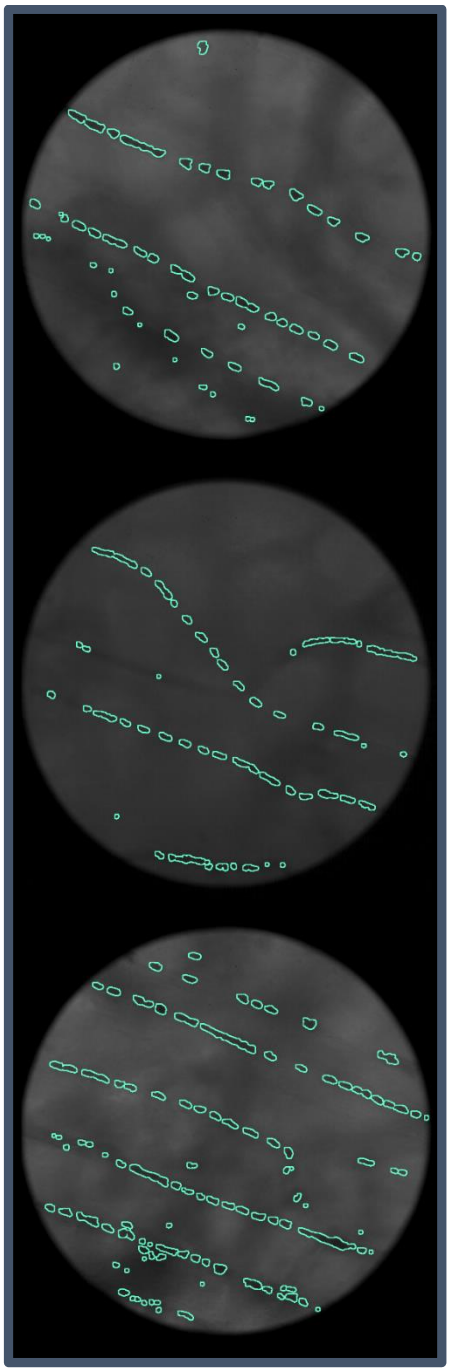

Figure 3: Video frames with erythrocyte contour lines overlaid.

Contour Segmentation

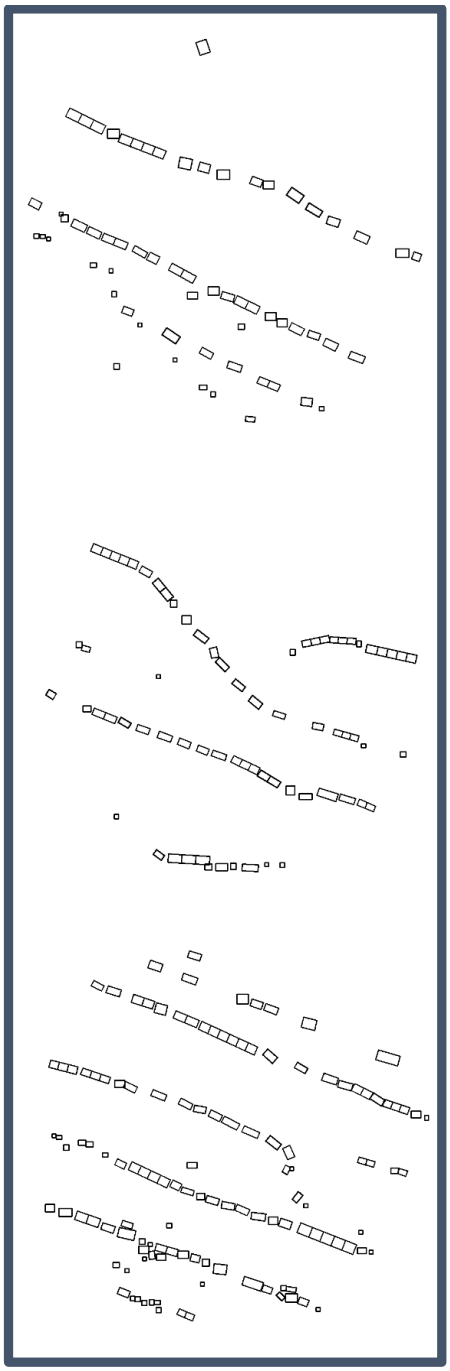

Figure 4: Segmented rectangular bounding boxes derived from video frames.

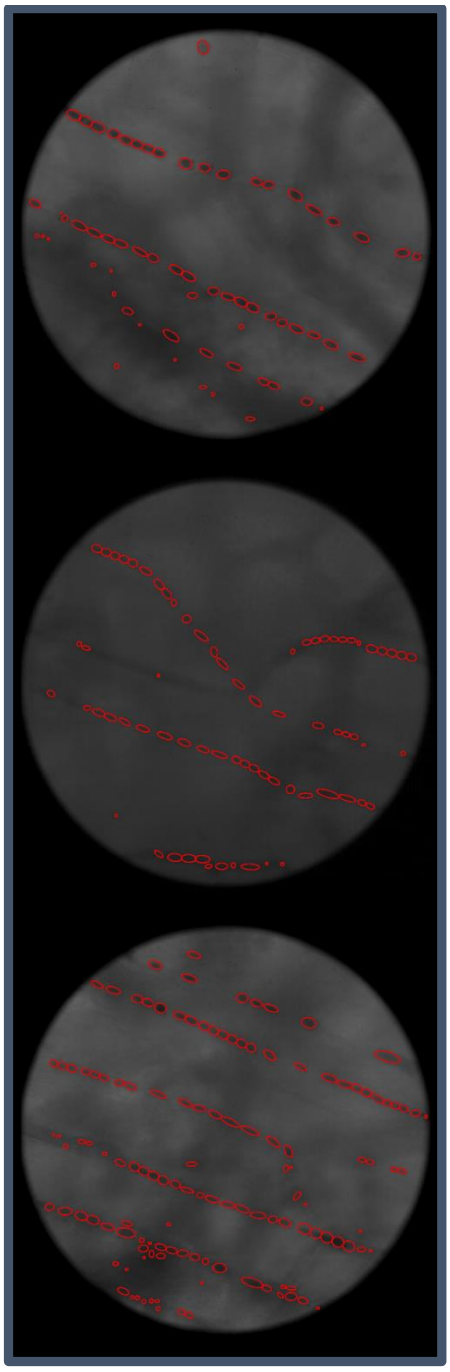

Figure 5: Video frames with erythrocyte placement approximations overlaid.

Capillary Segregation

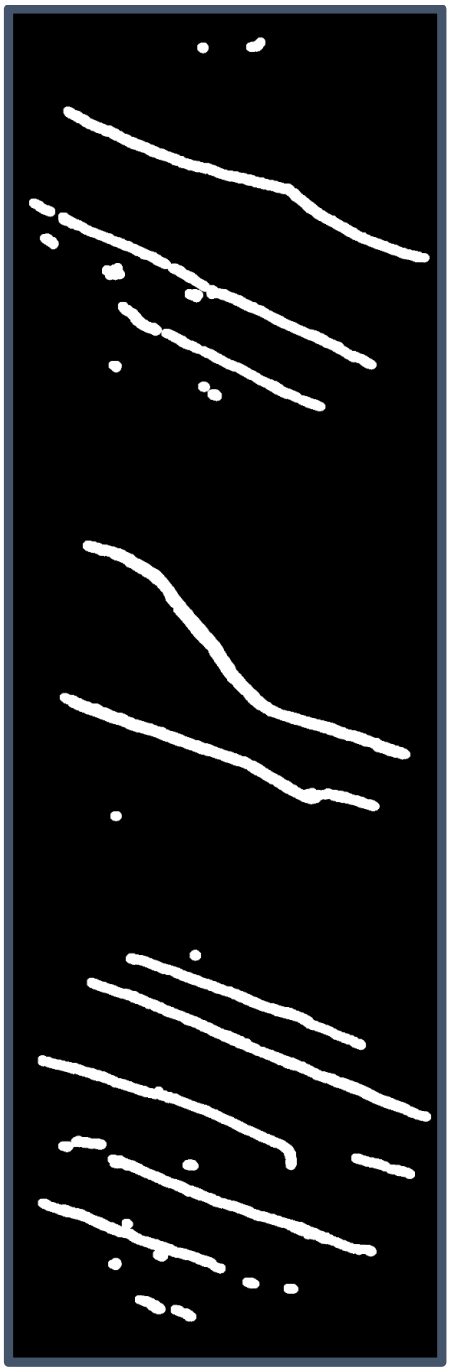

Figure 6: Masking images derived from capillary boundary estimation.

Outputs

The velocity of each cell is calculated by dividing the number of pixels along the path it traveled, as estimated previously using the smoothing algorithm, by the number of frames it was detected for. Knowing the frames per second of the input video, velocity is returned as a number of pixels traveled per second. The user will have to utilize outside information from the experimental set-up in order to convert this into a value of meaning for evaluation outside the context of the study. Values are averaged within capillary segments, weighted based on the total distance traveled by each included cell.

The average area per frame taken up by all cells within a capillary segment is divided by the area of that capillary segment to provide an estimation of capillary hematocrit.

The software can additionally be compiled in a manner that outputs all of the raw pathing data for each successfully tracked cell.

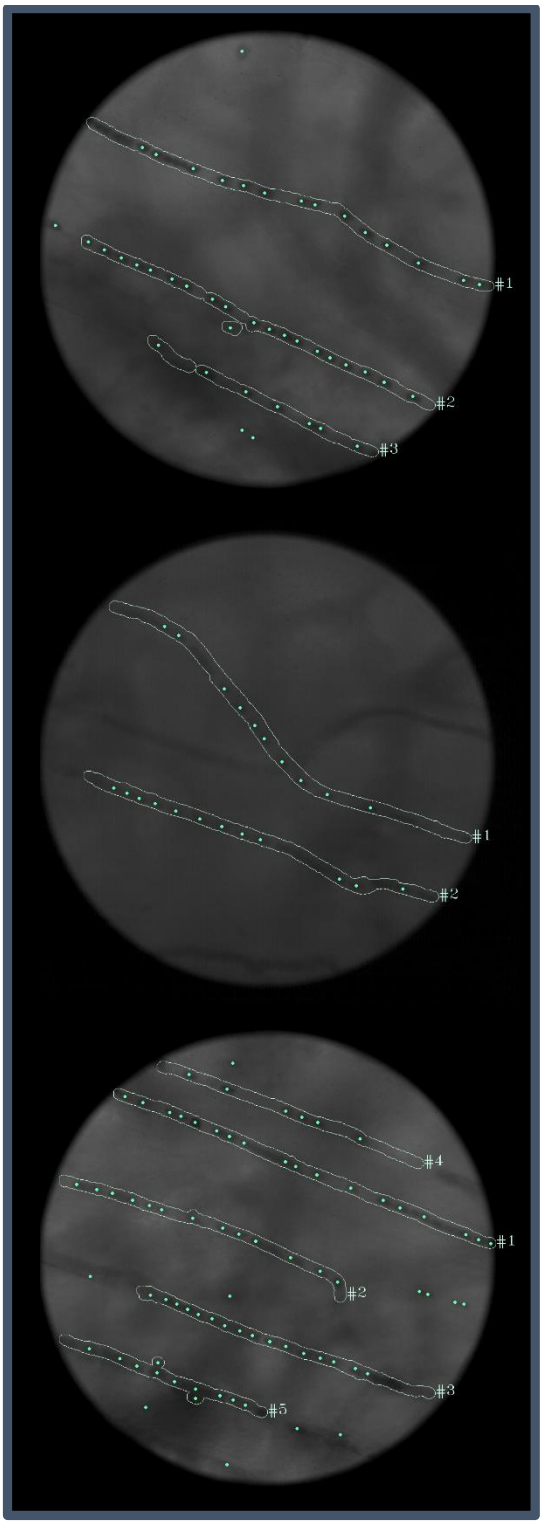

Figure 7: Video frames from the output file, with successfully tracked cells marked and capillary boundaries displayed.

IV: Discussion

The main advantage of this application is its ability to calculate a large quantity of data automatically. Once calibrated and assuming video samples are consistent, a user may compile the software in a manner that lets it accept multiple arguments, allowing very large sample sizes covering representative areas of the microcirculation to be assessed. The emphasis on user control and self-validation are advantageous and presented in the form of optional raw data outputs and an output video file that allows the user to quickly assess what information was gathered.

Limitations

With the software attempting to assess capillaries specifically, other small vessels are left un-evaluated. Additionally, capillary hematocrit estimations are reliant on stable imagery and appropriate user input for dilation and erosion values. The amount of time it takes to analyze a given video is primarily dependent on video length and processor speed, meaning that slower computers will be at a disadvantage assessing large quantities of data. Furthermore, very high frame rates are required when acquiring videos so that erythrocyte position in one frame may be tied to the next with certainty. The software makes no attempt to analyze capillaries differently based on bifurcations, lumping velocity and hematocrit values together should they belong within the same contour region.

V: Conclusion

Given the vital role that capillaries play in delivering oxygen to critical organ systems, being able to analyze changes in microhemodynamics specific to capillaries could lead to advancements in our understanding and treatment of diseases like sepsis. This software presents itself as a small step forward in that direction.

Future Directions

There are a large number of studies that could stand to benefit by including capillary-specific data as a supplement to standard methods of microcirculatory assessment such as functional capillary density. As processor speeds improve, the software can be compiled in a manner that permits real-time analysis and tracking, permitting experimental interventional therapies to take place in response to microcirculatory changes quickly in the laboratory setting.

References

1 Adhikari, N. K., Fowler, R. A., Bhagwanjee, S. & Rubenfeld, G. D. Critical care and the global burden of critical illness in adults. *The Lancet* **376**, 1339-1346 (2010).

2 Torio, C. M. & Andrews, R. M. National inpatient hospital costs: the most expensive conditions by payer, 2011. (2013).

3 Lagu, T. Hospitalizations, costs, and outcomes of severe sepsis in the United States 2003 to 2007. *Critical care medicine* **40**, 754-761 (2012).

4 Stevenson, E. K., Rubenstein, A. R., Radin, G. T., Wiener, R. S. & Walkey, A. J. Two decades of mortality trends among patients with severe sepsis: a comparative meta-analysis. *Critical care medicine* **42**, 625 (2014).

5 Gaieski, D. F., Edwards, J. M., Kallan, M. J. & Carr, B. G. Benchmarking the incidence and mortality of severe sepsis in the United States*. *Critical care medicine* **41**, 1167-1174 (2013).

6 Weil, M. H. & Shubin, H. The VIP approach to the bedside management of shock. *JAMA* **207**, 337-340 (1969).

7 Hotchkiss, R. S. & Karl, I. E. The pathophysiology and treatment of sepsis. *New England Journal of Medicine* **348**, 138-150 (2003).

8 Dellinger, R. P. Surviving Sepsis Campaign: international guidelines for management of severe sepsis and septic shock, 2012. *Intensive care medicine* **39**, 165-228 (2013).

9 Ince, C. & Sinaasappel, M. Microcirculatory oxygenation and shunting in sepsis and shock. *Critical care medicine* **27**, 1369-1377 (1999).

10 Spronk, P. E., Zandstra, D. F. & Ince, C. Bench-to-bedside review: sepsis is a disease of the microcirculation. *Critical care* **8**, 462 (2004).

11 De Backer, D., Durand, A. & Donadello, K. Microcirculation alterations in patients with severe sepsis. *Clinical pulmonary medicine* **22**, 31-35 (2015).

12 Sakr, Y., Dubois, M.-J., De Backer, D., Creteur, J. & Vincent, J.-L. Persistent microcirculatory alterations are associated with organ failure

and death in patients with septic shock*. *Critical care medicine* **32**, 1825-1831 (2004).

13 Wells Jr, R. E. Rheology of blood in the microvasculature. *New England Journal of Medicine* **270**, 832-839 (1964).

14 Andrade, L. E. C., Gabriel, A., Assad, R. L., Ferrari, A. J. L. & Atra, E. in *Seminars in arthritis and rheumatism*. 21-31 (Elsevier).

15 Ingegnoli, F. Prognostic model based on nailfold capillaroscopy for identifying Raynaud's phenomenon patients at high risk for the development of a scleroderma spectrum disorder: PRINCE (prognostic index for nailfold capillaroscopic examination). *Arthritis & Rheumatism* **58**, 2174-2182 (2008).

16 Mannarino, E., Pasqualini, L., Fedeli, F., Scricciolo, V. & Innocente, S. Nailfold capillaroscopy in the screening and diagnosis of Raynaud's phenomenon. *Angiology* **45**, 37-42 (1994).

17 Groner, W. Orthogonal polarization spectral imaging: a new method for study of the microcirculation. *Nature medicine* **5**, 1209-1212 (1999).

18 Erol-Yilmaz, A. Cardiac resynchronization improves microcirculation. *Journal of cardiac failure* **13**, 95-99 (2007).

19 Nivoit, P., Wiernsperger, N., Moulin, P., Lagarde, M. & Renaudin, C. Effect of glycated LDL on microvascular tone in mice: a comparative study with LDL modified in vitro or isolated from diabetic patients. *Diabetologia* **46**, 1550-1558 (2003).

20 Weidlich, K. Changes in microcirculation as early markers for infection in preterm infants—an observational prospective study. *Pediatric research* **66**, 461-465 (2009).

21 Černý, V. Orthogonal polarization spectral imaging. *Physiol Res* **56**, 141-147 (2007).

22 Lindert, J. OPS imaging of human microcirculation: a short technical report. *Journal of vascular research* **39**, 368-372 (2002).

23 Ince, C. Sidestream dark field imaging: an improved technique to observe sublingual microcirculation. *Critical care* **9**, 1-1 (2005).

24 Elbers, P. W., Ozdemir, A., van Iterson, M., van Dongen, E. P. & Ince, C. Microcirculatory imaging in cardiac anesthesia: ketanserin reduces blood pressure but not perfused capillary density. *Journal of cardiothoracic and vascular anesthesia* **23**, 95-101 (2009).

25 Milstein, D. M., Bezemer, R., Lindeboom, J. A. & Ince, C. The acute effects of CMF-based chemotherapy on maxillary periodontal microcirculation. *Cancer chemotherapy and pharmacology* **64**, 1047-1052 (2009).

26 Goedhart, P., Khalilzada, M., Bezemer, R., Merza, J. & Ince, C. Sidestream Dark Field (SDF) imaging: a novel stroboscopic LED ring-based imaging modality for clinical assessment of the microcirculation. *Optics express* **15**, 15101-15114 (2007).

27 Mouthon, M.-A., Vereycken-Holler, V., Van der Meeren, A. & Gaugler, M.-H. Irradiation increases the interactions of platelets with the endothelium in vivo: analysis by intravital microscopy. (2009).

28 Jain, R. K., Munn, L. L. & Fukumura, D. Dissecting tumour pathophysiology using intravital microscopy. *Nature Reviews Cancer* **2**, 266-276 (2002).

29 Sumen, C., Mempel, T. R., Mazo, I. B. & von Andrian, U. H. Intravital microscopy: visualizing immunity in context. *Immunity* **21**, 315-329 (2004).

30 Hughes, E. L. & Gavins, F. N. Troubleshooting methods: using intravital microscopy in drug research. *Journal of pharmacological and toxicological methods* **61**, 102-112 (2010).

31 Lee, E. J., Rosenbaum, J. T. & Planck, S. R. Epifluorescence intravital microscopy of murine corneal dendritic cells. *Investigative ophthalmology & visual science* **51**, 2101 (2010).

32 Bos, G., Majoor, G., Slaaf, D., Reneman, R. & van Breda, V. P. In vivo demonstration of microvascular pathology by intravital microscopy in experimental chronic graft-versus-host disease: analogy with scleroderma. *The Journal of rheumatology* **15**, 1339-1345 (1988).

33 Hickman, H. D., Bennink, J. R. & Yewdell, J. W. Caught in the act: intravital multiphoton microscopy of host-pathogen interactions. *Cell host & microbe* **5**, 13-21 (2009).

34 Menger, M. D., Laschke, M. W. & Vollmar, B. Viewing the microcirculation through the window: some twenty years experience with the hamster dorsal skinfold chamber. *European Surgical Research* **34**, 83-91 (2002).

35 De Backer, D., Creteur, J., Preiser, J.-C., Dubois, M.-J. & Vincent, J.-L. Microvascular blood flow is altered in patients with sepsis. *American journal of respiratory and critical care medicine* **166**, 98-104 (2002).

36 De Backer, D. How to evaluate the microcirculation: report of a round table conference. *Critical care* **11**, R101 (2007).

37 Boerma, E. C., Mathura, K. R., van der Voort, P. H., Spronk, P. E. & Ince, C. Quantifying bedside-derived imaging of microcirculatory abnormalities in septic patients: a prospective validation study. *Critical Care* **9**, R601 (2005).

38 Spronk, P. E. Nitroglycerin in septic shock after intravascular volume resuscitation. *The lancet* **360**, 1395-1396 (2002).

39 Petersen, S. M., Greisen, G., Hyttel-Sorensen, S. & Hahn, G. H. Sidestream dark field images of the microcirculation: intra-observer reliability and correlation between two semi-quantitative methods for determining flow. *BMC medical imaging* **14**, 14 (2014).

40 Pozo, M. O., Kanoore Edul, V. S., Ince, C. & Dubin, A. Comparison of different methods for the calculation of the microvascular flow index. *Critical care research and practice* **2012** (2012).

41 Klyscz, T., Jünger, M., Jung, F. & Zeintl, H. Cap image--a new kind of computer-assisted video image analysis system for dynamic capillary microscopy. *Biomedizinische Technik. Biomedical engineering* **42**, 168-175 (1997).

42 Schaudig, S., Dadasch, B., Kellam, K. & Christ, F. in *Proceedings of the 7th World Congress for Microcirculation.* 2-59.

43 Endrich, B., Asaishi, K., Götz, A. & Meßmer, K. Technical report—a new chamber technique for microvascular studies in unanesthetized hamsters. *Research in Experimental Medicine* **177**, 125-134 (1980).

44 Suzuki, S. Topological structural analysis of digitized binary images by border following. *Computer Vision, Graphics, and Image Processing* **30**, 32-46 (1985).